

Titania/ C_n TAB Nanoskeleton as adsorbent and photocatalyst for removal of alkylphenols dissolved in water

Toshio Sakai,* Albar Da Loves, Tomohiko Okada, Shozi Mishima

Department of Chemistry and Material Engineering, Faculty of Engineering, Shinshu University, 4-17-1 Wakasato, Nagano 380-8553, Japan

* To whom correspondence should be addressed.

phone : +81-26-269-5405

fax : +81-26-269-5424

e-mail : tsakai@shinshu-u.ac.jp

Abstract

We report here on the removal of alkylphenols (phenol, 4-*n*-propylphenol, 4-*n*-heptylphenol and 4-nonylphenol) dissolved in water using the composite particles of nanocrystalline titania and alkyltrimethylammonium bromide ($C_nH_{2n+1}N(CH_3)_3Br$, C_nTAB ; $n = 12, 14, 16$ and 18) (named as TiO_2/C_nTAB Nanoskeleton) as adsorbents and photocatalysts. In particular, the adsorption of alkylphenols onto TiO_2/C_nTAB Nanoskeleton in water was investigated in terms of hydrophobic interaction between alkylphenols and C_nTAB , surface area, pore structure and crystal size of TiO_2/C_nTAB Nanoskeleton. We revealed that C_nTAB incorporated in the TiO_2/C_nTAB Nanoskeleton promotes the adsorption of alkylphenols onto TiO_2/C_nTAB Nanoskeleton due to the hydrophobic interaction between alkylphenols and C_nTAB . On the other hand, the surface area, pore structure and crystal size of TiO_2/C_nTAB Nanoskeleton did not affect the adsorption of alkylphenols onto TiO_2/C_nTAB Nanoskeleton. We also found that the alkylphenols dissolved in water were completely removed by the combination of adsorption and photocatalytic degradation by the TiO_2/C_nTAB Nanoskeleton under UV irradiation. These results prove that the TiO_2/C_nTAB Nanoskeleton acts as in tandem an adsorbent and a photocatalyst for removal of alkylphenols dissolved in water.

Key Words : Adsorption, Photocatalysis, Titania Nanoskeleton, Alkyltrimethylammonium bromide, Alkylphenols

1. Introduction

Removal of chemical contaminants from wastewater continues to be a critical issue in environmental remediation. Several techniques such as adsorption, reverse osmosis, biological degradation, chemical oxidation, precipitation and electro dialysis are applied to remove the chemical contaminants from wastewater [1-29]. Adsorption is considered as one of the effective and versatile methods. For example, activated carbon is one of the most popular sorbent materials to extract chemical contaminants from wastewater. In recent years, organic/inorganic hybrid porous materials such as organic molecules-grafted mesoporous materials have attracted attention as effective adsorbents for removal of organic contaminants from water [5-13]. In addition, several reports describe that mesoporous silica materials (MCM-41) containing surfactant template also act as effective adsorbents for the removal of organic contaminants from aqueous solutions [14-21]. In the organic/inorganic hybrid adsorbents, inorganic parts act as adsorption substrate and provide large surface area. Organic parts add the adsorption-ability and -selectivity to the inorganic substrates. Furthermore, combining of titania (TiO_2) with organic/inorganic hybrid porous materials is expected to enhance the removal of organic contaminants from water due to the synergistic effect of adsorption and photocatalytic degradation of organic contaminants [22-29].

Then, we considered to apply the composite particles of nanocrystalline titania (anatase) and alkyltrimethylammonium bromide ($\text{C}_n\text{H}_{2n+1}\text{N}(\text{CH}_3)_3\text{Br}$, C_nTAB ; $n = 12, 14, 16$ and 18) (named as $\text{TiO}_2/\text{C}_n\text{TAB}$ Nanoskeleton) that we have recently developed [30-32] as adsorbents and photocatalysts for adsorption and degradation of organic contaminants. The $\text{TiO}_2/\text{C}_n\text{TAB}$ Nanoskeleton should extract organic contaminants from water due to the solubilization of organic contaminants into

C_n TAB domain incorporated in the TiO_2/C_n TAB Nanoskeleton and to degrade organic contaminants due to the photocatalysis of nanocrystalline titania in TiO_2/C_n TAB Nanoskeleton.

In this paper, we examine the potential of the TiO_2/C_n TAB Nanoskeleton as adsorbent and photocatalyst for removal of organic contaminants dissolved in water. The TiO_2/C_n TAB Nanoskeleton was prepared through sol-gel reaction of titanium oxysulfate sulfuric acid hydrate ($TiOSO_4 \cdot xH_2SO_4 \cdot xH_2O$, TiOSAH) initiated by C_n TAB spherical micelles in an aqueous solution in the absence of any other additives such as acid and base [30-32]. Compared with the synthetic methods reported [33-35], our synthetic system involves benefits such as (i) spontaneous formation of hexagonally ordered pore-structure through simple procedure (mixing of aqueous solutions containing TiOSAH and C_n TAB but no other additives such as acid and base as reaction initiators required, (ii) crystallization of titania (anatase formation) in aqueous solutions under mild condition (e.g., at 60 °C for 24 h), (iii) no evaporation and calcination processes required for formation of ordered pore-structure and crystallization of titania and (iv) utilization of water as a solvent [30-32]. This matches with recent emerging environmental requirements on nanomaterial synthetic strategy such as a simplified procedure, minimized material use, low energy input and utilization of environmentally benign solvents.

2. Experimental

2.1. Preparation of TiO_2/C_n TAB Nanoskeleton

Hexagonal-structured TiO_2/C_n TAB Nanoskeleton (denoted as HX-TNS- n) was prepared through sol-gel reaction of a 3.0 mol L⁻¹ titanium oxysulfate sulfuric acid hydrate ($TiOSO_4 \cdot xH_2SO_4 \cdot xH_2O$, TiOSAH; Aldrich) aqueous solution (18.2 mΩ cm,

Millipore-filtered water) at 60 °C for 24 h initiated by mixing of an aqueous solution containing $60 \times 10^{-3} \text{ mol L}^{-1}$ alkyltrimethylammonium bromide ($\text{CH}_3(\text{CH}_2)_n\text{N}^+(\text{CH}_3)_3\text{Br}^-$, C_nTAB , $n = 12, 14, 16$ and 18 ; Aldrich) (following the procedure that we have reported previously) [30-32]. Precipitates thus produced were filtrated and washed by water, and finally, the powder of the HX-TNS- n was obtained after drying at 120 °C for 10 h under air atmosphere. Alkyltrimethylammonium bromide (C_nTAB , $n = 12, 14, 16$ and 18) was used to investigate the effect of hydrocarbon chain length of C_nTAB on the adsorption of alkylphenols onto HX-TNS- n . Role of C_nTAB on adsorption of alkylphenols onto $\text{TiO}_2/\text{C}_n\text{TAB}$ Nanoskeleton was also investigated by comparison with the adsorption of alkylphenols onto calcined HX-TNS- n at 450 °C for 2 h (denoted as CA-TNS- n), in which C_nTAB was removed from HX-TNS- n by calcination. Moreover, $\text{TiO}_2/\text{C}_n\text{TAB}$ Nanoskeleton with higher specific surface area and lower content of C_nTAB (denoted as SC-TNS- n) was prepared to check the connections between alkylphenol adsorption, surface area and C_nTAB content in the $\text{TiO}_2/\text{C}_n\text{TAB}$ Nanoskeleton. The SC-TNS- n was prepared through sol-gel reaction of a 3.0 mol L^{-1} TiOSAH aqueous solution mixed with a $60 \times 10^{-3} \text{ mol L}^{-1}$ C_nTAB aqueous solution at 100 °C for 72 h. Powder of the SC-TNS- n was obtained through same procedure with that of HX-TNS- n .

2.2 Characterization of HX-TNS- n , CA-TNS- n and SC-TNS- n

Pore structure, crystal type and crystallinity of the HX-TNS- n , CA-TNS- n and SC-TNS- n were characterized using powder X-ray diffraction (XRD) system (RINT-2200V PC, RIGAKU). For example, three peaks assigned to hexagonally ordered pore-structure ($d_{100} : d_{110} : d_{200} = 1 : 1/\sqrt{3} : 1/2$)[32] in low-angle region (see **Figure 1a**) and a XRD pattern assigned to anatase titania ((101), (004), (200), (105) and

(211) facets of anatase)[36, 37] (see **Figure 1a'**) were observed in the HX-TNS-16. A broad peak of XRD assigned to (100) facet in low-angle region (see **Figure 1b**) and a XRD pattern assigned to anatase titania ((101), (004), (200), (105) and (211) facets of anatase) in wide-angle region (see **Figure 1b'**) were observed in CA-TNS-16 that was obtained after calcination of the HX-TNS-16. In the case of SC-TNS-16, no noticeable peak was observed in low-angle region of XRD pattern (see **Figure 1c**), indicating that there is no ordered pore-structure in the SC-TNS-16. The XRD pattern observed in wide-angle region for the SC-TNS-16 was assigned to anatase titania ((101), (004), (200), (105) and (211) facets of anatase) (see **Figure 1c'**). Pore structure and crystal type of HX-TNS-*n*, CA-TNS-*n* and SC-TNS-*n* (*n* = 12, 14 and 18) are same with those of HX-TNS-16, CA-TNS-16 and SC-TNS-16. Value of *d*-spacing estimated from XRD pattern of HX-TNS-*n* increased as the diameter of C_{*n*}TAB micelles (hydrocarbon chain length of C_{*n*}TAB), suggesting that C_{*n*}TAB micelles act as templates for the formation of hexagonally ordered pore-structure. Pore structure, *d*-spacing, crystal type and crystal size of the HX-TNS-*n*, CA-TNS-*n* and SC-TNS-*n* obtained from the XRD measurements were summarized in **Table 1**. Morphology and nanostructure of HX-TNS-*n*, CA-TNS-*n* and SC-TNS-*n* were confirmed by scanning electron microscopy (SEM) (VE-9800, KEYENCE, 20 kV) and transmission electron microscopy (TEM) (JEM-2010, JEOL, 200 kV, 3.0 μA). For example, the HX-TNS-16 was micron-sized agglomerate (see **Figures 2a and 3a**) containing the honeycomb-like structure with the pore diameter of 2.9 nm (average diameter) and framework (wall) thickness of 1.2 nm (average thickness) (see **Figure 3a'**). Sum of the pore diameter and framework thickness was in good agreement with the value of *d*₁₀₀-spacing (3.97 nm) (distance between pores = pore diameter + framework thickness) estimated from the (100) peak of low-angle XRD (see **Table 1**).

Also pore diameter of HX-TNS-16 is consistent with micelle diameter (see **Table 1**). This supports that C₁₆TAB micelles act as templates for the formation of hexagonally ordered pore-structure of HX-TNS-16. The CA-TNS-16 was micron-sized agglomerate (see **Figures 2b and 3b**) which was constructed by the aggregation of nanometer-sized particles (the diameter of ~5 nm) (see **Figure 3b'**). The SC-TNS-16 was submicron-sized particles (see **Figures 2c and 3c**) which were aggregates of nanometer-sized particles (the diameter of ~5 nm) (see **Figure 3c'**). Similar images were observed in HX-TNS-*n*, CA-TNS-*n* and SC-TNS-*n* (*n* = 12, 14 and 18). Specific surface areas of the TiO₂/C_{*n*}TAB Nanoskeleton and CA-TNS-*n* determined using Brunauer, Emmett, Teller (BET) method (BELSORP-miniII, BEL JAPAN) were listed in **Table 1**. Presence of C_{*n*}TAB in TiO₂/C_{*n*}TAB Nanoskeleton and CA-TNS-*n* was confirmed by measuring the absorption bands (2850-2950 cm⁻¹) originating from stretching vibration of CA-H with FT-IR spectrometer (FT/IR-4200, JASCO). Also contents of C_{*n*}TAB in the TiO₂/C_{*n*}TAB Nanoskeleton and CA-TNS-*n* determined from weight loss measured with the simultaneous thermogravimetry/differential thermal analysis (TG/DTA) measurements (DTG-50H, SHIMADZU) (heating rate of 1 °C min⁻¹ under air atmosphere) were also listed in **Table 1**.

2.3 Adsorption properties of alkylphenols onto HX-TNS-*n*, CA-TNS-*n* and SC-TNS-*n*

Adsorption of alkylphenols (Phenol, C₆H₅OH; 4-*n*-propylphenol, CH₃(CH₂)₂C₆H₄OH; 4-*n*-heptylphenol, CH₃(CH₂)₆C₆H₄OH; 4-nonylphenol, CH₃(CH₂)₈C₆H₄OH; Tokyo Chemical Industry Co., Ltd.) onto HX-TNS-*n*, CA-TNS-*n* and SC-TNS-*n* was examined as follows: Powder (5 mg) of HX-TNS-*n*, CA-TNS-*n*

and SC-TNS-*n* was dispersed in a 1.5×10^{-5} mol L⁻¹ alkylphenol aqueous solution (50 mL) by ultrasonication (28 kHz). The dispersion was left standing under dark condition, and concentration of residual alkylphenol in water was estimated from absorbance (centered at ~190 nm) originating from alkylphenol measured with UV-visible spectrophotometer (U-1900, HITACHI) after centrifugation of the powder. Solubility of phenol, 4-*n*-propylphenol, 4-*n*-heptylphenol and 4-nonylphenol at 25 °C is 8.84×10 g L⁻¹, 1.28 g L⁻¹, 1.22×10^{-2} g L⁻¹ and 5.43×10^{-3} g L⁻¹, respectively [38].

2.3 Photocatalytic activities of HX-TNS-*n*, CA-TNS-*n* and SC-TNS-*n*

Photocatalytic activities of HX-TNS-*n*, CA-TNS-*n* and SC-TNS-*n* were determined in terms of 4-*n*-heptylphenol degradation under UV irradiation (LED-100UV365STND, 365 nm, 2 mW cm⁻², OPTOCODE CORPORATION) after adsorption of 4-*n*-heptylphenol onto HX-TNS-16, CA-TNS-16 and SC-TNS-16 under dark condition for 24 h. Concentration of residual 4-*n*-heptylphenol in water was estimated from absorbance (centered at ~190 nm) originating from 4-*n*-heptylphenol measured with UV-visible spectrophotometer (U-1900, HITACHI) after centrifugation of the powder.

3. Results and Discussion

3.1 Role of C_{*n*}TAB in TiO₂/C_{*n*}TAB Nanoskeleton on adsorption of alkylphenols

Surfactant micelles are small containers that can capture and store organic compounds dissolved in aqueous solutions [39]. Thus, surfactant micelles are one of the effective soft materials to extract the organic contaminants from aqueous solutions. However, it is not easy to separate the surfactant micelles solubilizing the organic contaminants from aqueous solutions due to the nanometer-sized and soft materials.

So, micron-sized inorganic materials combining with surfactants are considered as effective adsorbents to extract organic contaminants from aqueous solutions [14-21]. Then, we applied the $\text{TiO}_2/\text{C}_n\text{TAB}$ Nanoskeleton [30-32] as adsorbent for removal of alkylphenols from aqueous solutions. Namely, we considered that alkylphenols dissolved in water would be removed by $\text{TiO}_2/\text{C}_n\text{TAB}$ Nanoskeleton due to the solubilization of alkylphenols into $\text{TiO}_2/\text{C}_n\text{TAB}$ Nanoskeleton. Indeed, the concentration of residual alkylphenols in water decreased with the elapsed time after mixing of HX-TNS-16 powder with aqueous alkylphenol solutions but not CA-TNS-16 (see **Figure 4**). That is, alkylphenols dissolved in water adsorbed onto HX-TNS-16 but not onto CA-TNS-16. This indicates that C_{16}TAB incorporated in HX-TNS-16 contributes to the removal of alkylphenols from water. This also implies that C_{16}TAB incorporated in HX-TNS-16 acts as adsorption sites for alkylphenols dissolved in water. We also noticed that amount of alkylphenols adsorbed onto HX-TNS- n increased with hydrophobicity of alkylphenols (with the order of phenol < 4- n -propylphenol < 4- n -heptylphenol < 4- n -nonylphenol). This supports that hydrophobic interaction between alkylphenols and adsorbents is a critical factor for adsorption of organic compounds onto adsorbents.

3.2 Selectivity of alkylphenols adsorbed onto $\text{TiO}_2/\text{C}_n\text{TAB}$ Nanoskeleton

Now we realized that adsorption of alkylphenols onto HX-TNS-16 was caused by hydrophobic interaction between alkylphenols and C_{16}TAB in the HX-TNS-16. As mentioned in previous section (section 3.1), alkylphenols with higher hydrophobicity preferred to adsorb onto HX-TNS-16 (see **Figure 4**). This brings us an idea that different hydrophobicity of C_nTAB incorporated in HX-TNS- n should exhibit different adsorption-ability and -selectivity of alkylphenols. Then, HX-TNS- n

synthesized using C_n TAB with different hydrocarbon chain length was applied to elucidate the connection between hydrophobicity of C_n TAB in HX-TNS- n and adsorption of alkylphenols onto HX-TNS- n . In the case of HX-TNS-12, 4- n -heptylphenol and 4-nonylphenol adsorbed onto HX-TNS-12 but phenol and 4- n -propylphenol did not (see **Figure 5a**). Amount of 4- n -heptylphenol and 4-nonylphenol adsorbed onto HX-TNS-12 increased with hydrophobicity of alkylphenols (4- n -heptylphenol < 4-nonylphenol). Amount of 4- n -heptylphenol and 4-nonylphenol adsorbed onto HX-TNS-14 was larger than that onto HX-TNS-12 while phenol and 4- n -propylphenol did not adsorb onto HX-TNS-14 as well as HX-TNS-12 (see **Figure 5b**). The HX-TNS-16 and HX-TNS-18 adsorbed 4- n -propylphenol, 4- n -heptylphenol and 4-nonylphenol but not phenol (see **Figure 5c and d**). Amount of 4- n -propylphenol, 4- n -heptylphenol and 4-nonylphenol adsorbed onto HX-TNS-18 was larger than those onto HX-TNS-16. These results obviously indicate that adsorption of alkylphenols onto HX-TNS- n was controlled by hydrophobicity of C_n TAB incorporated in HX-TNS- n . This also suggests that alkylphenols were selectively removed by tuning the hydrophobicity of HX-TNS- n .

3.3 Role of surface area of TiO_2/C_n TAB Nanoskeleton on adsorption of alkylphenols

Having established the role of C_n TAB in the HX-TNS- n on the adsorption of alkylphenols dissolved in water, our interest turns into the connection between surface area of TiO_2/C_n TAB Nanoskeleton and adsorption of alkylphenols, because, in general, mesoporous materials act as effective adsorbents and substrates for catalysts due to their high specific surface area [1-29]. Then, we examined the adsorption of alkylphenols onto SC-TNS- n which has higher specific surface area and lower C_n TAB

content than HX-TNS-*n* (see **Table 1**) to confirm the effect of surface area of TiO₂/C_{*n*}TAB Nanoskeleton on the adsorption of alkylphenols onto TiO₂/C_{*n*}TAB Nanoskeleton. Concentration of alkylphenols in water decreased with the elapsed time after mixing of SC-TNS-*n* powder with aqueous alkylphenol solutions (see **Figure 6**), indicating that SC-TNS-*n* enables to extract alkylphenols from water. Compared with the amounts of alkylphenols adsorbed onto HX-TNS-*n* (see **Figures 5 and 6**), the amounts of alkylphenols removed by the SC-TNS-*n* were smaller than those by HX-TNS-*n*. This implies that amounts of alkylphenols adsorbed onto TiO₂/C_{*n*}TAB Nanoskeleton are determined by content of C_{*n*}TAB incorporated in the TiO₂/C_{*n*}TAB Nanoskeleton but not by surface area of TiO₂/C_{*n*}TAB Nanoskeleton (see **Table 1**). This result also suggests that pore structure of TiO₂/C_{*n*}TAB Nanoskeleton is not related to the adsorption of alkylphenols onto TiO₂/C_{*n*}TAB Nanoskeleton. Namely, the content of C_{*n*}TAB incorporated in the TiO₂/C_{*n*}TAB Nanoskeleton is an important factor for removal of alkylphenols dissolved in water rather than surface area and pore structure of the TiO₂/C_{*n*}TAB Nanoskeleton. This supports that the adsorption of organic compound onto inorganic material requires not only surface area of the inorganic material but also interaction between organic compound and inorganic material. We confirmed that MCM-41 with high specific surface area (~1000 m² g⁻¹) did not capture the alkylphenols dissolved in water (the result is not reported here). Namely, if there is no significant interaction between organic compound and inorganic material, the organic compound would not adsorb onto the inorganic material even though the inorganic material has large surface area. We also confirmed that the crystal size of titania in the TiO₂/C_{*n*}TAB Nanoskeleton was not related to the adsorption of alkylphenols onto TiO₂/C_{*n*}TAB Nanoskeleton (see **Table 1**).

3.4 Photocatalytic degradation of alkylphenols by TiO₂/C_nTAB Nanoskeleton

Finally, photocatalytic activity of TiO₂/C_nTAB Nanoskeleton was checked in terms of alkylphenol degradation by TiO₂/C_nTAB Nanoskeleton. We expect that the organic contaminants adsorbed onto TiO₂/C_nTAB Nanoskeleton and residual organic contaminants in bulk solutions would be degraded by TiO₂/C_nTAB Nanoskeleton due to the photocatalysis of nanocrystalline titania. Indeed, every TiO₂/C_nTAB Nanoskeleton that we examined in this work enabled to degrade the alkylphenols dissolved in water, indicating that TiO₂/C_nTAB Nanoskeleton have photocatalytic activity. For example, 4-*n*-heptylphenols dissolved in water were degraded by HX-TNS-16, CA-TNS-16 and SC-TNS-16 under UV irradiation (see **Figure 7**). Then, kinetics of 4-*n*-heptylphenol degradation by TiO₂/C_nTAB Nanoskeleton was discussed to evaluate the connection between adsorption and photocatalysis of TiO₂/C_nTAB Nanoskeleton. The Langmuir-Hinshelwood kinetic model developed for quantitative analysis of gaseous-solid reactions is now the most commonly used method of expressing the heterogeneous catalytic process. This is simplified to a first-order reaction and given as follows [40]:

$$-\ln\left(\frac{C}{C_0}\right) = k_{\text{app}} \cdot t \quad (1)$$

where C_0 is the initial concentration of the organic molecule, C is the concentration at any time during degradation (mg L^{-1}), k_{app} is the apparent rate constant and t is the irradiation time.

The apparent rate constants, k_{app} , of 4-*n*-heptylphenol degradation determined from the slope of the line obtained by plotting $-\ln(C/C_0)$ vs. t (time) were 0.017, 0.011 and 0.014 h^{-1} for HX-TNS-16, CA-TNS-16 and SC-TNS-16, respectively. Namely, the photocatalysis of $\text{TiO}_2/\text{C}_{16}\text{TAB}$ Nanoskeleton for 4-*n*-heptylphenol degradation increases with the order of CA-TNS-16 < SC-TNS-16 < HX-TNS-16. This order is consistent with the amount of 4-*n*-heptylphenols adsorbed onto $\text{TiO}_2/\text{C}_{16}\text{TAB}$ Nanoskeleton (CA-TNS-16 < SC-TNS-16 < HX-TNS-16) (see **Figure 7**). This supports that the photocatalysis of $\text{TiO}_2/\text{C}_{16}\text{TAB}$ Nanoskeleton for the degradation of 4-*n*-heptylphenols is enhanced by the adsorption of 4-*n*-heptylphenols onto the $\text{TiO}_2/\text{C}_{16}\text{TAB}$ Nanoskeleton. We also found that the photocatalysis of $\text{TiO}_2/\text{C}_{16}\text{TAB}$ Nanoskeleton for the degradation of 4-*n*-heptylphenol was not related to the crystal size of titania (see **Table 1**) while larger crystal of titania generally enhances the photocatalytic activity. This also supports that the interaction between organic compound and titania material is required for the enhancement of titania photocatalysis.

4. Conclusions

We investigated the potential of $\text{TiO}_2/\text{C}_n\text{TAB}$ Nanoskeleton as adsorbent and photocatalyst for removal of organic contaminants from water. The $\text{TiO}_2/\text{C}_n\text{TAB}$ Nanoskeleton enabled to remove alkylphenols by adsorption and photocatalysis. Adsorption of alkylphenols by $\text{TiO}_2/\text{C}_n\text{TAB}$ Nanoskeleton was dominated by hydrophobic interaction between alkylphenols and C_nTAB incorporated in the $\text{TiO}_2/\text{C}_n\text{TAB}$ Nanoskeleton. Amounts of alkylphenols removed by $\text{TiO}_2/\text{C}_n\text{TAB}$ Nanoskeleton were determined in terms of C_nTAB content incorporated in the $\text{TiO}_2/\text{C}_n\text{TAB}$ Nanoskeleton rather than surface area, pore structure and crystal size of

TiO₂/C_nTAB Nanoskeleton. We also proved that combination of adsorption with photocatalysis promoted the removal of alkylphenols from water. These findings would provide better insight on the designing of adsorbents and development of environmental remediation systems by means of adsorption.

Acknowledgments

This study was performed through Program for Dissemination of Tenure Tracking System funded by the Ministry of Education and Science, Japan. We are grateful to the Japan Aerospace Exploration Agency (Grant JDX-2005185A) and Nippon Sheet Glass Foundation for Materials Science and Engineering for support of this research.

References

- [1] A. Fujishima, X. Zhang, D.A. Tryk, Heterogeneous photocatalysis: From water photolysis to applications in environmental cleanup, *Int. J. Hydrogen Energy* 32 (2007) 2664-2672.
- [2] G. Busca, S. Berardinelli, C. Resini, L. Arrighi, Technologies for the removal of phenol from fluid streams: A short review of recent developments, *J. Hazard. Mater.* 160 (2008) 265-288.
- [3] M. Ahmaruzzaman, Adsorption of phenolic compounds on low-cost adsorbents: A review, *Adv. Colloid Interface Sci.* 143 (2008) 48-67.
- [4] S.H. Lin, R.S. Juang, Adsorption of phenol and its derivatives from water using synthetic resins and low-cost natural adsorbents: A review, *J. Environ. Manag.* 90 (2009) 1336-1349.
- [5] A. Stein, B.J. Melde, R.C. Schrodin, Hybrid inorganic-organic mesoporous silicates - Nanoscopic reactors coming of age, *Adv. Mater.* 12 (2000) 1403-1419.
- [6] Y.F. Lu, H.Y. Fan, N. Doke, D.A. Loy, R.A. Assink, D.A. LaVan, C.J. Brinker, Evaporation-induced self-assembly of hybrid bridged silsesquioxane film and particulate mesophases with integral organic functionality, *J. Am. Chem. Soc.* 122 (2000) 5258-5261.
- [7] A. Sayari, S. Hamoudi, Periodic mesoporous silica-based organic-inorganic nanocomposite materials, *Chem. Mater.* 13 (2001) 3151-3168.
- [8] D.J. Yang, Y. Xu, D. Wu, Y.H. Sun, H.Y. Zhu, F. Deng, Super hydrophobic mesoporous silica with anchored methyl groups on the surface by a one-step synthesis without surfactant template, *J. Phys. Chem. C* 111 (2007) 999-1004.
- [9] K. Inumaru, Y. Inoue, S. Kakii, T. Nakano, S. Yamanaka, Molecular selective

adsorption of dilute alkylphenols and alkylanilines from water by alkyl-grafted MCM-41: tunability of the cooperative organo-inorganic function in the nanostructure, *Phys. Chem. Chem. Phys.* 6 (2004) 3133-3139.

[10] K. Inumaru, T. Nakano, S. Yamanaka, Molecular selective adsorption of alkylphenols and alkylanilines from water by alkyl-grafted mesoporous alumina: A comparative study to alkyl-grafted mesoporous silica, *Micropor. Mesopor. Mater.* 95 (2006) 279-285.

[11] H.Y. Huang, C.L. Yang, H.X. Zhang, M.C. Liu, Preparation and characterization of octyl and octadecyl-modified mesoporous SBA-15 silica molecular sieves for adsorption of dimethyl phthalate and diethyl phthalate, *Micropor. Mesopor. Mater.* 111 (2008) 254-259.

[12] Q. Hu, J.J. Li, Z.P. Hao, L.D. Li, S.Z. Qiao, Dynamic adsorption of volatile organic compounds on organofunctionalized SBA-15 materials, *Chem. Eng. J.* 149 (2009) 281-288.

[13] J.G. He, K. Ma, J. Jin, Z.P. Dong, J.J. Wang, R. Li, Preparation and characterization of octyl-modified ordered mesoporous carbon CMK-3 for phenol adsorption, *Micropor. Mesopor. Mater.* 121 (2009) 173-177.

[14] R. Denoyel, E.S. Rey, Solubilization in confined surfactant mesophases, *Langmuir* 14 (1998) 7321-7323.

[15] K. Hanna, I. Beurroies, R. Denoyel, D. Desplandier-Giscard, A. Galarneau, F. Di Renzo, Sorption of hydrophobic molecules by organic/inorganic mesostructures, *J. Colloid Interface Sci.* 252 (2002) 276-283.

[16] K. Hanna, R. Denoyel, I. Beurroies, Compared solubilisation properties of bulk micelles and confined surfactant phases, *Colloids Surf. A* 248 (2004) 33-41.

[17] K. Hanna, R. Denoyel, I. Beurroies, J.P. Dubes, Solubilization of

pentachlorophenol in micelles and confined surfactant phases, *Colloids Surf. A* 254 (2005) 231-239.

[18] Y. Miyake, M. Hanaeda, M. Asada, Separation of organic compounds by spherical mesoporous silica prepared from W/O microemulsions of tetrabutoxysilane, *Ind. Eng. Chem. Res.* 46 (2007) 8152-8157.

[19] L. Huang, Q.L. Huang, H.N. Xiao, M. Eic, Effect of cationic template on the adsorption of aromatic compounds in MCM-41, *Micropor. Mesopor. Mater.* 98 (2007) 330-338.

[20] P.A. Mangrulkar, S.P. Kamble, J. Meshram, S.S. Rayalu, Adsorption of phenol and o-chlorophenol by mesoporous MCM-41, *J. Hazard. Mater.* 160 (2008) 414-421.

[21] X.X. Yang, Q.X. Guan, W. Li, Effect of template in MCM-41 on the adsorption of aniline from aqueous solution, *J. Environ. Manag.* 92 (2011) 2939-2943.

[22] K. Mogyorosi, A. Farkas, I. Dekany, I. Ilisz, A. Dombi, TiO₂-based photocatalytic degradation of 2-chlorophenol adsorbed on hydrophobic clay, *Environ. Sci. Technol.* 36 (2002) 3618-3624.

[23] T. Kasahara, K. Inumaru, S. Yamanaka, Enhanced photocatalytic decomposition of nonylphenol polyethoxylate by alkyl-grafted TiO₂-MCM-41 organo-inorganic nanostructure, *Micropor. Mesopor. Mater.* 76 (2004) 123-130.

[24] K. Inumaru, M. Murashima, T. Kasahara, S. Yamanaka, Enhanced photocatalytic decomposition of 4-nonylphenol by surface-organografted TiO₂: a combination of molecular selective adsorption and photocatalysis, *Appl. Catal. B* 52 (2004) 275-280.

[25] K. Inumaru, T. Kasahara, M. Yasui, S. Yamanaka, Direct nanocomposite of crystalline TiO₂ particles and mesoporous silica as a molecular selective and highly active photocatalyst, *Chem. Commun.* (2005) 2131-2133.

- [26] X.L. Zhu, C.W. Yuan, H.L. Chen, Photocatalytic degradation of pesticide pyridaben. 3. In surfactant/TiO₂ aqueous dispersions, *Environ. Sci. Technol.* 41 (2007) 263-269.
- [27] Y. Shiraishi, Y. Sugano, D. Inoue, T. Hirai, Effect of substrate polarity on photocatalytic activity of titanium dioxide particles embedded in mesoporous silica, *J. Catal.* 264 (2009) 175-182.
- [28] Y. Kuwahara, K. Maki, Y. Matsumura, T. Kamegawa, K. Mori, H. Yamashita, Hydrophobic Modification of a Mesoporous Silica Surface Using a Fluorine-Containing Silylation Agent and Its Application as an Advantageous Host Material for the TiO₂ Photocatalyst, *J. Phys. Chem. C* 113 (2009) 1552-1559.
- [29] Y. Kuwahara, J. Aoyama, K. Miyakubo, T. Eguchi, T. Kamegawa, K. Mori, H. Yamashita, TiO₂ photocatalyst for degradation of organic compounds in water and air supported on highly hydrophobic FAU zeolite: Structural, sorptive, and photocatalytic studies, *J. Catal.* 285 (2012) 223-234.
- [30] H. Shibata, T. Ogura, T. Mukai, T. Ohkubo, H. Sakai, M. Abe, Direct synthesis of mesoporous titania particles having a crystalline wall, *J. Am. Chem. Soc.* 127 (2005) 16396-16397.
- [31] H. Shibata, H. Mihara, T. Mukai, T. Ogura, H. Kohno, T. Ohkubo, H. Sakai, M. Abe, Preparation and formation mechanism of mesoporous titania particles having crystalline wall, *Chem. Mater.* 18 (2006) 2256-2260.
- [32] T. Sakai, H. Yano, M. Ohno, H. Shibata, K. Torigoe, S. Utsumi, K. Sakamoto, N. Koshikawa, S. Adachi, H. Sakai, M. Abe, Formation mechanism for hexagonal-structured self-assemblies of crystalline titania templated by cetyltrimethylammonium bromide, *J. Oleo Sci.* 57 (2008) 629-637.
- [33] A. Corma, From microporous to mesoporous molecular sieve materials and

their use in catalysis, *Chem. Rev.* 97 (1997) 2373-2419.

[34] G.J.A.A. Soler-Illia, C. Sanchez, B. Lebeau, J. Patarin, Chemical strategies to design textured materials: From microporous and mesoporous oxides to nanonetworks and hierarchical structures, *Chem. Rev.* 102 (2002) 4093-4138.

[35] G.J.D.A. Soler-Illia, E.L. Crepaldi, D. Grosso, C. Sanchez, Block copolymer-templated mesoporous oxides, *Curr. Opin. Colloid Interface Sci.* 8 (2003) 109-126.

[36] H. Zhang, J.F. Banfield, Kinetics of crystallization and crystal growth of nanocrystalline anatase in nanometer-sized amorphous titania, *Chem. Mater.* 14 (2002) 4145-4154.

[37] H.P. Klug, L.E. Alexander, *X-Ray Diffraction Procedures For Polycrystalline and Amorphous Materials*, John Wiley & Sons, Inc., New York, 1974.

[38] D. Varhanickova, W.Y. Shiu, D. Mackay, Aqueous solubilities of alkylphenols and methoxyphenols at 25 °C, *J. Chem. Eng. Data* 40 (1995) 448-451.

[39] D.F. Evans, H. Wennerstrom, *THE COLLOIDAL DOMAIN Where Physics, Chemistry, Biology, and Technology Meet* Second Edition, WILEY-VCH, New York, 1999.

[40] K.V. Kumar, K. Porkodi, F. Rocha, Langmuir-Hinshelwood kinetics - A theoretical study, *Catal. Commun.* 9 (2008) 82-84.

Table 1. Properties of HX-TNS-*n*, CA-TNS-*n* and SC-TNS-*n*

Sample	Micelle diameter (nm)	C _n TAB content (wt%)	Pore structure	d _{hkl} (nm)			Crystal type	Crystal size (nm)	N ₂ -adsorption and desorption isotherm	BET surface area (m ² g ⁻¹)
				d ₁₀₀	d ₁₁₀	d ₂₀₀				
HX-TNS-12	1.9	38	Hexagonal	3.44	2.08	1.69	Anatase	3.06	II	2.1
CA-TNS-12		3.6	No ordered structure	-	-	-	Anatase	5.06	IV	15.6
SC-TNS-12		10	No ordered structure	-	-	-	Anatase	18.3	II	187.7
HX-TNS-14	2.2	47	Hexagonal	3.69	2.21	1.89	Anatase	2.12	II	2.8
CA-TNS-14		2.0	No ordered structure	-	-	-	Anatase	1.50	IV	23.5
SC-TNS-14		11	No ordered structure	-	-	-	Anatase	19.2	II	104.3
HX-TNS-16	2.6	49	Hexagonal	3.97	2.31	1.99	Anatase	7.67	II	2.0
CA-TNS-16		2.7	No ordered structure	3.07	-	-	Anatase	6.80	IV	65.4
SC-TNS-16		13	No ordered structure	-	-	-	Anatase	19.6	II	66.9
HX-TNS-18	3.1	55	Hexagonal	4.59	2.66	2.33	Anatase	0.44	II	2.3
CA-TNS-18		2.2	No ordered structure	-	-	-	Anatase	12.38	IV	23.0
SC-TNS-18		14	No ordered structure	-	-	-	Anatase	21.7	II	54.7

Figure captions

Figure 1. Low-angle XRD and wide-angle XRD patterns of (Panels a and a') HX-TNS-16, (Panels b and b') CA-TNS-16 and (Panels c and c') SC-TNS-16.

Figure 2. SEM images of (image a) HX-TNS-16, (image b) CA-TNS-16 and (image c) SC-TNS-16.

Figure 3. TEM images of (images a and a') HX-TNS-16, (images b and b') CA-TNS-16 and (images c and c') SC-TNS-16.

Figure 4. Residual ratios (C/C_0) of alkylphenols (●: phenol, ○: 4-*n*-propylphenol, ■: 4-*n*-heptylphenol, □: 4-nonylphenol) in water plotted as a function of elapsed time. C_0 and C are concentrations of alkylphenols in water before and after mixing of Nanoskeleton powder with alkylphenols aqueous solutions, respectively. (Panel a) HX-TNS-16 and (Panel b) CA-TNS-16.

Figure 5. Residual ratios (C/C_0) of alkylphenols (●: phenol, ○: 4-*n*-propylphenol, ■: 4-*n*-heptylphenol, □: 4-nonylphenol) in water plotted as a function of elapsed time. C_0 and C are concentrations of alkylphenols in water before and after mixing of HX-TNS-*n* powder with alkylphenols aqueous solutions, respectively. (Panel a) HX-TNS-12, (Panel b) HX-TNS-14, (Panel c) HX-TNS-16 and (Panel d) HX-TNS-18.

Figure 6. Residual ratios (C/C_0) of alkylphenols (●: phenol, ○: 4-*n*-propylphenol, ■: 4-*n*-heptylphenol, □: 4-nonylphenol) in water plotted as a function of elapsed time.

C_0 and C are concentrations of alkylphenols in water before and after mixing of SC-TNS- n powder with alkylphenols aqueous solutions, respectively. (Panel a) SC-TNS-12, (Panel b) SC-TNS-14, (Panel c) SC-TNS-16 and (Panel d) SC-TNS-18.

Figure 7. Residual ratios (C/C_0) of 4- n -heptylphenol in water plotted as a function of elapsed time. C_0 and C are concentrations of 4- n -heptylphenol in water before and after mixing of Nanoskeleton powder with 4- n -heptylphenol aqueous solutions, respectively. Decreases in C/C_0 from 0 to 24 h and from 24 to 120 h represent the adsorption of 4- n -heptylphenol onto Nanoskeleton powder under dark condition and photocatalytic degradation of 4- n -heptylphenol by Nanoskeleton powder under UV irradiation. (■) HX-TNS-16, (●) SC-TNS-16, (□) CA-TNS-16 and (○) control solution (4- n -heptylphenol aqueous solution).

Figure 1. Sakai et al.

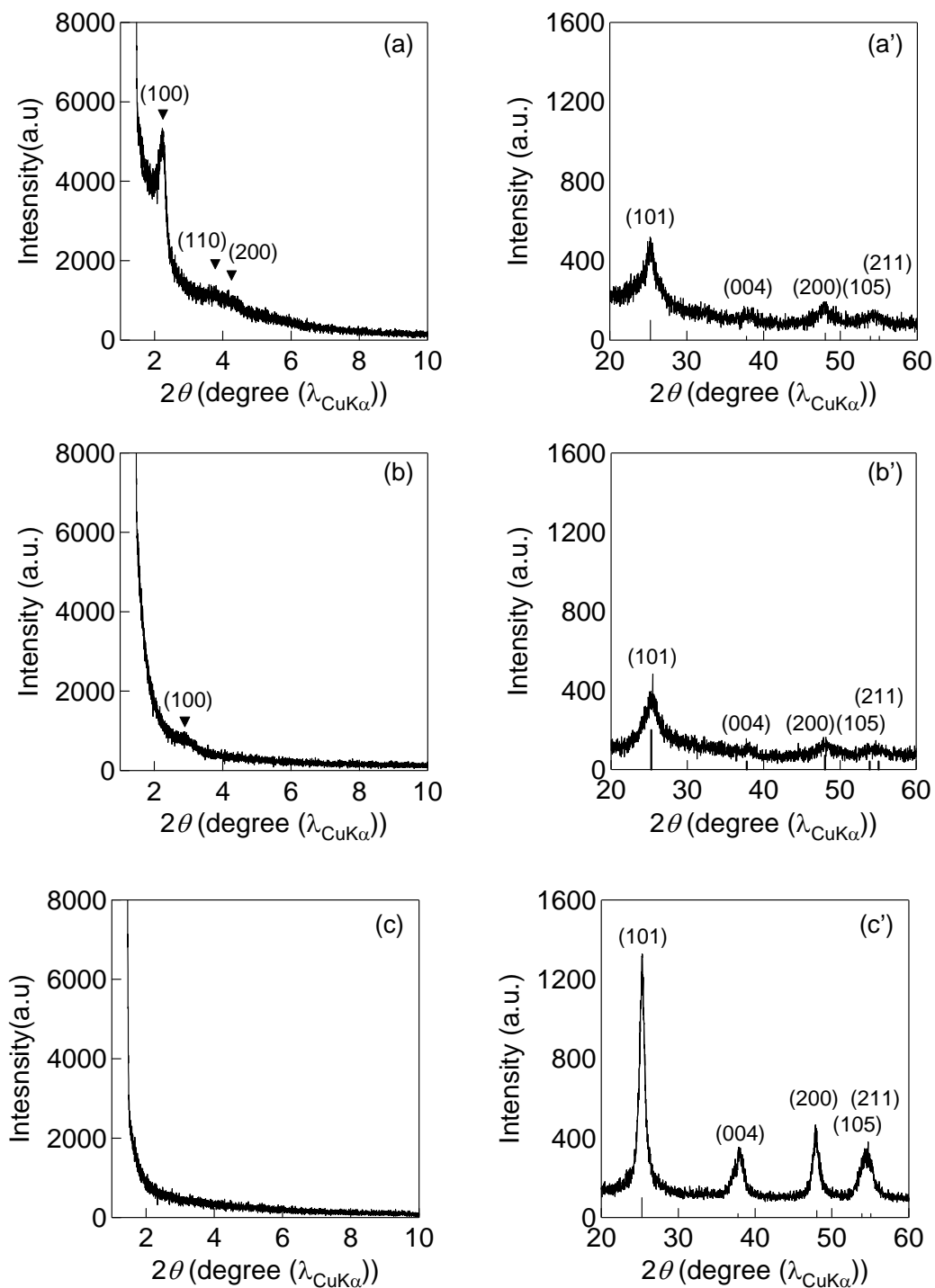


Figure 2. Sakai et al.

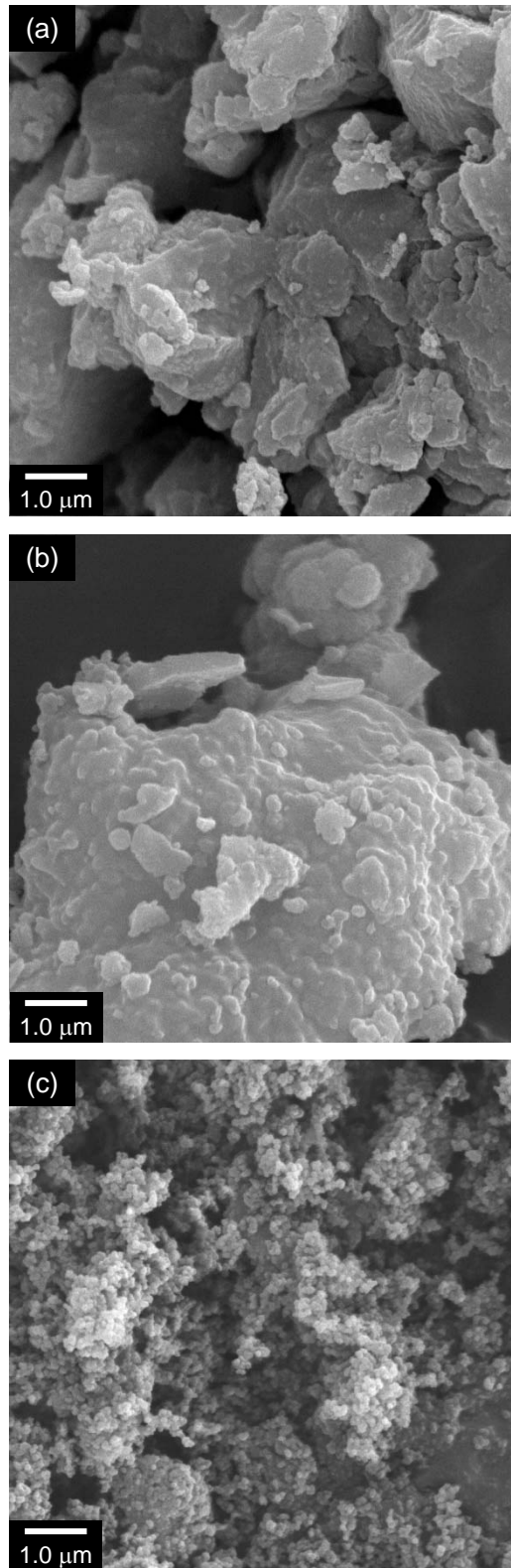


Figure 3. Sakai et al.

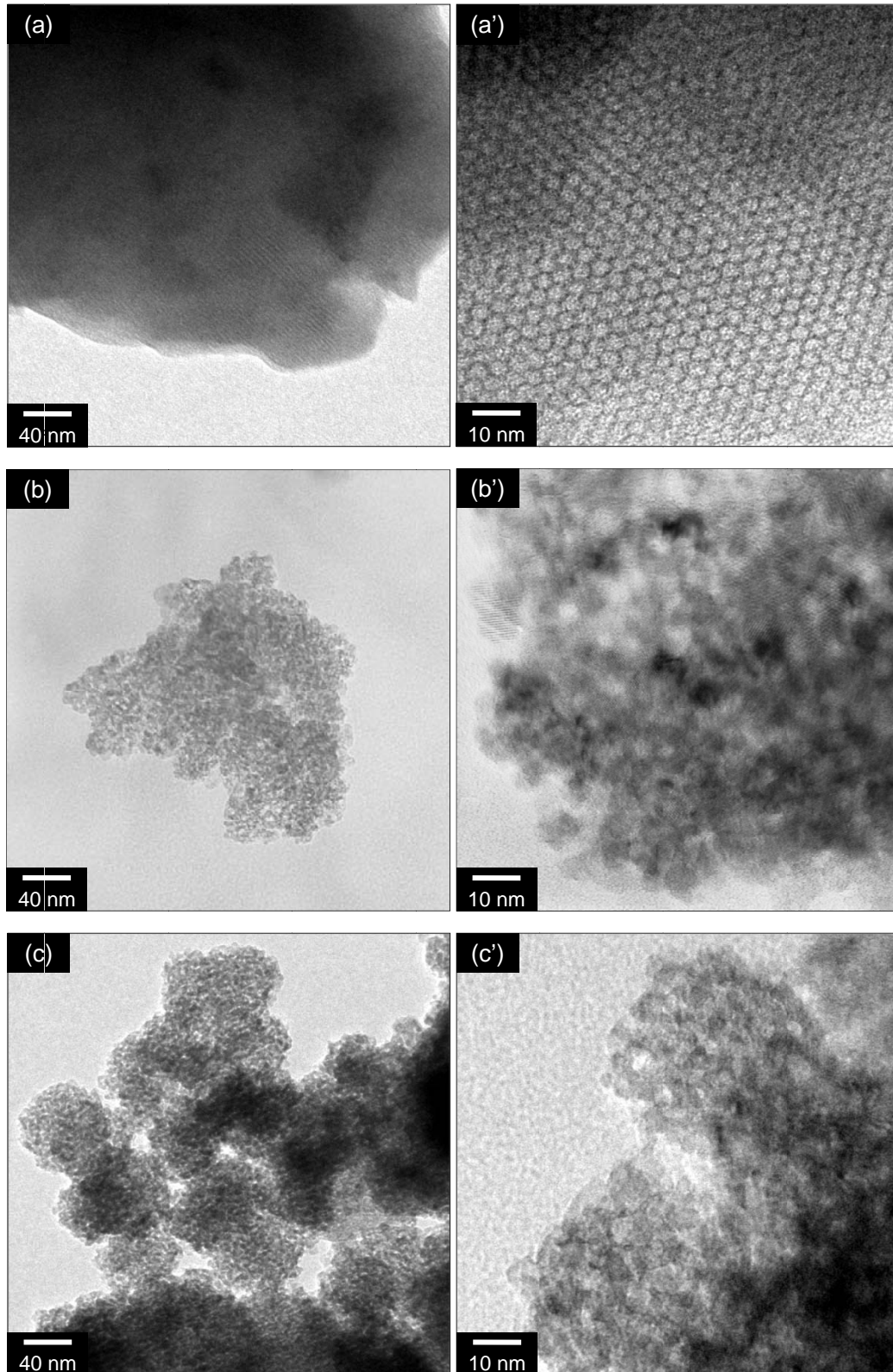


Figure 4. Sakai et al.

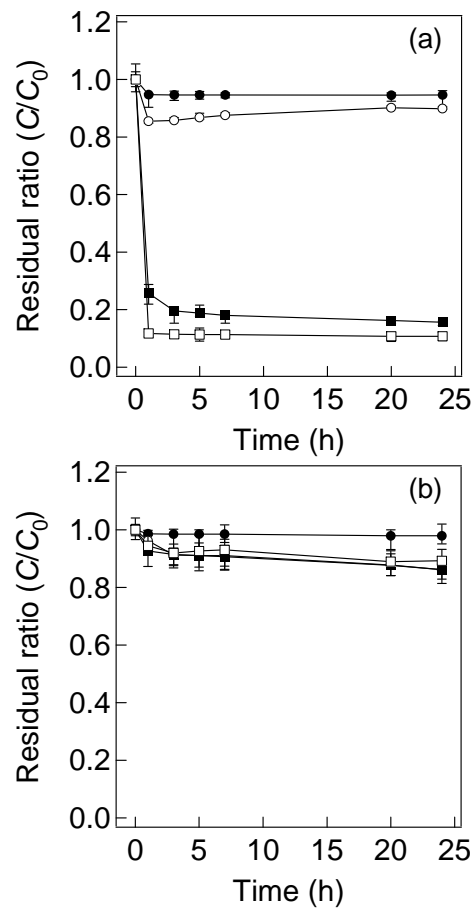


Figure 5. Sakai et al.

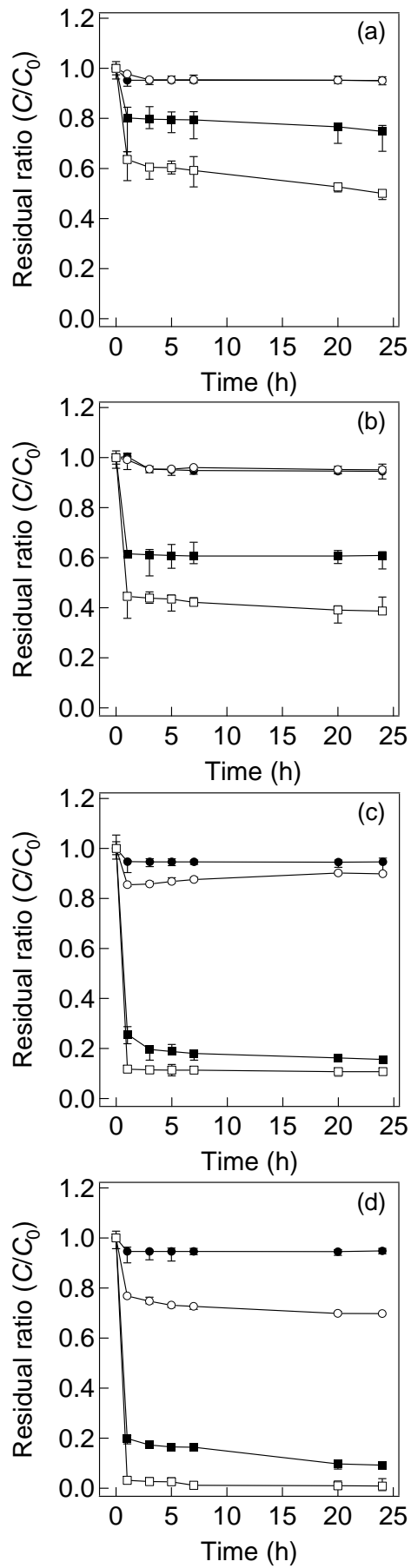


Figure 6. Sakai et al.

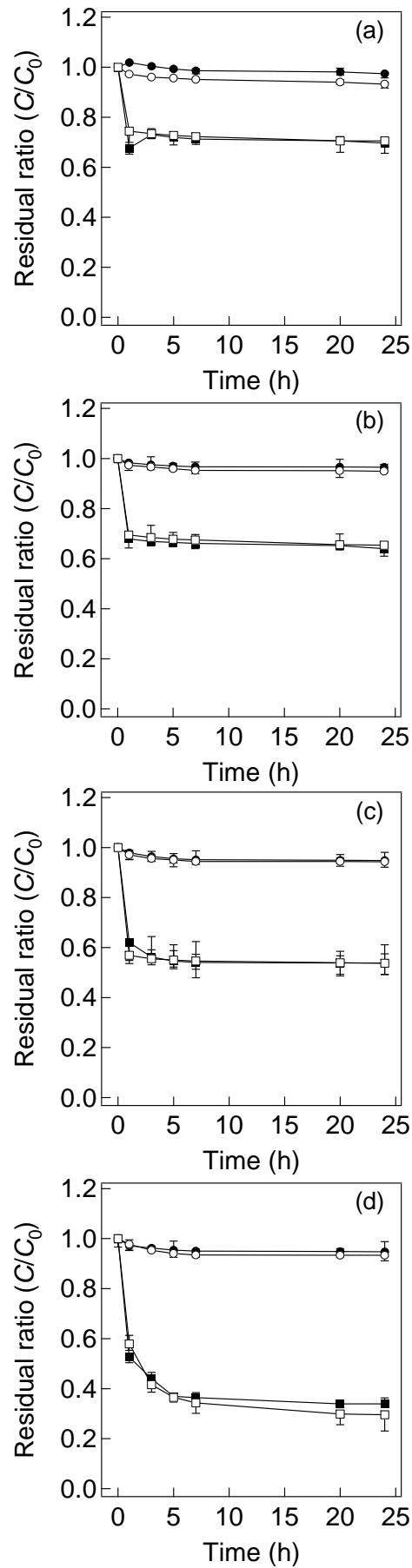


Figure 7. Sakai et al.

